Eur. Phys. J. D (2015) 69: 78
DOI: 10.1140/epjd/e2015-50766-7

THE EUROPEAN PHYSICAL JOURNAL D

Regular Article

Electron collisions with H_2CNH using the R-matrix method

Kedong Wang[1,a], Ju Meng[1], and K.L. Baluja[2,b]

[1] College of Physics and Electronic Engineering, Henan Normal University, Xinxiang 453007, P.R. China
[2] Department of Physics and Astrophysics, University of Delhi, 110007 Delhi, India

Received 22 October 2014 / Received in final form 11 January 2015
Published online 19 March 2015 –

Abstract. The R-matrix approach is used to calculate the elastic differential, integral, and momentum transfer cross sections for electron impact on H_2CNH within static-exchange-polarization (SEP) and close-coupling (CC) approximations. The electron-impact excitation cross sections from the ground state to the first three low-lying electronic excited states of H_2CNH molecule have been also studied for the first time. A shape resonance of $^2A''$ symmetry located at 1.95 eV with a width of 0.56 eV is detected within CC model. The effective collision frequencies over a wide electron temperature range (200−30 000 K) are calculated using the data of the momentum-transfer cross section.

1 Introduction

Electron-molecule collisions are the dominant process in cool plasmas and discharges. These processes can also take place naturally in atmosphere through auroras [1] and lightning [2]. Besides planetary auroras [3], electron collisions initiate much of the chemistry found in the interstellar medium [4] and shocks [5]. Hotter regions in the interstellar medium, such as shocks [5] and planetary nebulae [6], are also influenced. The study of low-energy electron scattering from biological molecules helps to understand the effect of radiation on biological systems [7]. Due to difficulty in accurate representation of the target wave function, it remains a computational challenge for the accurate simulation of electron-molecule scattering at low scattering energies. As the simplest member of the imine family of compounds, methyleneimine (H_2CNH) possess a carbonnitrogen double bond. It is of interest in astrophysics and has been observed in dark interstellar dust clouds [8,9] and in Titan's upper atmosphere [10]. It has also been identified in the CO_2 laser-assisted decomposition of RDX at 0.1 to 3 atm [11]. Therefore, the investigation of electron interaction with H_2CNH not only provide the cross sections, but also may help in understanding of chemistry in atmosphere and in the radiation damage in biological systems.

The present work studies the low-energy electron scattering of methyleneimine molecule in the fixed-nuclei approximation using the UK molecular R-matrix code [12,13]. The R-matrix method has an advantage over other scattering methods because it can provide cross sections at a large number of scattering energies efficiently. It also has the ability to include correlation effects and give an adequate representation of several excited states of the molecule. Our interest lies in the low-energy region (0−10 eV), which is a favorite ground for the R-matrix method. The electron-scattering calculations are performed at static-exchange-polarization (SEP) and close-coupling approximations (CC). We have included ten target states in the CC approximations. The integrated elastic, differential, and momentum cross sections for electron impact on the methyleneimine molecule are reported. The excited cross sections from the ground state to a few low-lying excited states have also been calculated.

2 Method

2.1 Theory

In the present work we have employed the R-matrix method, which is an accurate procedure for low-energy electron scattering studies [14]. The hallmark of R-matrix methodology is that the R-matrix basis set is energy-independent. This implies diagonalising $(N + 1)$ electron Hamiltonian only once. Since the energy of the incident electron appears only in the denominator in the definition of R-matrix, which becomes a meromorphic function of energy. This greatly increases the speed with which cross sections can be computed over a fine energy mesh for subsequent analysis of any resonances that may appear. The method works on the principle of division of the configuration space into two spatial regions: inner and outer regions. The inner region radius is chosen to be $12a_0$, which can enclose almost all the electron cloud of target states and electron-target systems. In this region, the scattering electron is indistinguishable from the electrons of the target and the electron correlation and exchange are strong.

[a] e-mail: wangkd@htu.cn
[b] e-mail: kl_baluja@yahoo.com

Table 1. The vertical excitation energies (in eV) for the target states of H_2CNH. Ground-state dipole moments of μ value calculated in the present work are also given (in a.u.).

State	This work					MCSCF	SCF-CI	CSECI[a]	EHP[a]	Exp[b]
	6-31G	6-31++G**	cc-pVDZ	aug-cc-pVDZ	cc-pVTZ					
$1\,^1A'$	0	0	0	0	0	0	0	0	0	
$1\,^3A''$	4.34	4.72	4.71	5.13	4.83			3.82	4.57	
$1\,^3A'$	4.98	5.08	5.12	5.22	5.12			8.04	9.59	
$1\,^1A''$	5.02	5.33	5.42	5.68	5.49	5.44[c], 4.98[d]	5.83[e]	5.16	5.84	
$2\,^3A'$	8.63	7.55	8.56	8.03	8.33					
$2\,^1A'$	9.43	7.61	9.05	8.07	8.64			8.51	10.33	
$2\,^3A''$	9.75	8.84	9.63	9.19	9.59			4.03		
$2\,^1A''$	10.20	8.87	10.17	9.20	10.12			9.55		
$3\,^3A''$	11.30	9.59	10.71	9.72	10.34					
$3\,^1A''$	11.68	9.76	10.92	9.74	10.47					
$\mu(1^1A')$	0.691	0.634	0.548	0.567	0.555					0.787

[a]From reference [18], [b]from reference [17], [c]from reference [19], [d]from reference [20], [e]from reference [21].

The wave function of the scattering system is written using the configuration interaction (CI) expression

$$\Psi_k^{N+1} = \mathrm{A}\sum_{ij} a_{ijk}\Phi_i^N\left(x_1,\ldots,x_N\right)u_{ij}\left(x_{N+1}\right) + \sum_i b_{ik}\chi_i^{N+1}\left(x_1,\ldots,x_{N+1}\right), \quad (1)$$

where A is an antisymmetrization operator, x_N is the spatial and spin coordinate of the Nth electron, Φ_i^N represents the ith state of the N-electron target, μ_{ij} is a continuum-orbital spin coupled with the scattering electron, and k refers to a particular R-matrix basis function. Coefficients a_{ijk} and b_{ik} are variational parameters determined as a result of the matrix diagonalization. The sum in the second term of equation (1) represents the short-range correlation and polarization effects, running over all configurations χ_i^{N+1} that are L^2 functions. These are also important for relaxing the orthogonality imposed between the target and continuum orbitals.

In the outer region exchange between the scattering electron and electrons of the target is neglected and a single centre expansion of the electron-molecule interaction is used. The R-matrix is constructed and propagated to a radius ($\sim 100a_0$) large enough so that an asymptotic expansion for the radial wavefunctions of the scattering electron in each channel can be used.

In the present calculation the target molecular obital space is divided into core (inactive), valence (active), and virtual orbitals. These target molecular obitals are supplemented with a set of continuum orbitals, centered on the center of mass of the molecule. In the polyatomic R-matrix calculations, the continuum orbitals are Gaussian-type orbitals (GTOs). The main advantage of GTOs is that integrals involving them over all space can be evaluated analytically in closed form. First, Schmidt orthogonalization procedure is used to orthogonalize target and continuum molecule orbitals (MOs), then symmetric or Löwdin orthogonalization is used to orthogonalize the continuum orbitals among themselves and remove linearly dependent functions [15,16]. In general, all calculations in this work are performed within the fixed-nuclei approximation, which is based on the assumption in which electronic, vibrational and rotational motions are uncoupled.

2.2 Target model

The methyleneimine is a close-shell molecule which has X^1A' ground state in the C_s point group. The structural parameters optimized at B3LYP/6-311 + G** level (three bonds of C-N = 1.267 Å, N-H = 1.023 Å and C-H = 1.091 Å, two angles of H-C-N = 118.9° and C-N-H = 111.0°) are used in the present calculations. They are in good agreement with the experimental results as reported in the computational chemistry comparison and benchmark database (CCCBDB) [17]. To obtain the accurate vertical excited energies and dipole moment, a series of calculations were performed using CI model with five different basis sets 6-31G, 6-31++G**, cc-pVDZ, aug-cc-pVDZ, and cc-pVTZ. The Hatree-Fock (HF) self-consistent field (SCF) calculations for the ground state of methyleneimine were performed to obtain the occupied and virtual orbitals. These calculations at the different levels give the same electronic configuration at the ground state ($1a'^2 2a'^2 3a'^2 4a'^2 5a'^2 6a'^2 7a'^2 1a''^2$). In our CI model, eight frozen electrons were distributed in the $1a' \sim 4a'$ configuration. The remaining eight electrons are allowing to move freely in eight molecular orbitals ($5a' \sim 8a'$ and $1a'' \sim 4a''$) with the 6-31G basis set, and in eleven molecular orbitals with the other basis sets ($5a' \sim 9a'$ and $1a'' \sim 6a''$), respectively.

Table 1 lists the vertical excited energies (VEEs) and the ground state dipole moments at different levels together with the available experimental and theoretical data. As shown in the table, the 6-31G basis set gives a dipole moment (0.691 D) that is closest to the experimental value of 0.787 D [17]. Other larger basis sets even containing dispersion predict smaller dipole moment. 6-31G basis set also predicts the lower VEEs for the first three

excited states compared with other basis sets. Furthermore, we compare our calculated VEEs using 6-31G basis set with the available theoretical results. The first excited state $1^3A''$ is assigned to be the $\pi \rightarrow \pi^*$ transition, and the value of the VEE is 4.34 eV, which is 0.52 eV larger than the complete CI based on single excited configurations (CSECI) value [18] and 0.23 eV lower than electron-hole potential (EHP) value [18]. The VEE value of 4.98 eV for the second excited state $1^3A'$ ($n \rightarrow \sigma*$ transition) is much smaller than CSECI and EHP values. The VEE value of 5.02 eV for the third excited state $1^1A''$ ($n \rightarrow \pi^*$ transition) is smaller than the other available theoretical results including multiconfigurational SCF (MCSCF) [19,20], SCF-CI [21], CSECI [18] and EHP [18] methods. In summary, the calculations with the 6-31G basis set provide the best dipole moment and reliable vertical excitation energies. Then 6-31G basis set is adopted in the scattering calculations.

2.3 Scattering model

Two models are used in the present scattering calculation. The first model is the SEP model in which singlet excitations out of the HF wave function are used to represent target polarization effects. It can give the good resonance parameters for the shape resonant states. In the present calculations, the L^2 configurations in equation (1) associated with this model can be written in two classes, $(\text{core})^8(\text{valence})^8(\text{virtual})^1$ and $(\text{core})^8(\text{valence})^7(\text{virtual})^2$. In the present SEP model 13 MOs of A' symmetry ($8a' \sim 20a'$) and 3 MOs of A'' symmetry ($2a'' \sim 4a''$) are selected as virtual orbitals. The second model is the CC model in which many target states are included in the first sum of equation (1). These target states are usually performed by CI model. In the CC model, 10 target states are used to describe the electron plus target system. The L^2 configurations in equation (1) associated with this model can be written as, $(\text{core})^8(\text{CAS})^9$ and $(\text{core})^8(\text{CAS})^8(\text{virtual})^1$. Here the active space is composed of $5a' \sim 8a'$ and $1a'' \sim 4a''$ orbitals. The CC model is particularly good at representing the core-excited shape resonances and Feshbach resonances because the associated excited states of the target can be explicitly incorporated in the CC expansion. Another model is SE model which the target wave function is represented at the HF level and remains frozen during the collision process. We do not use SE model here for it can only give shape resonances that are usually too high in energy. It is noted that the CC calculations are more computationally expensive than the SE and SEP calculations.

The scattering calculations are carried out for doublet states with A' and A'' symmetries. The continuum orbitals up to g-partial waves are orthogonalized to the target orbitals based on the mixture of Schmidt and Löwdin symmetric orthogonalization [22] and represented by GTOs centered at the molecular center of gravity [15]. The continuum orbitals with an overlap of less than 2×10^{-7} are removed [15].

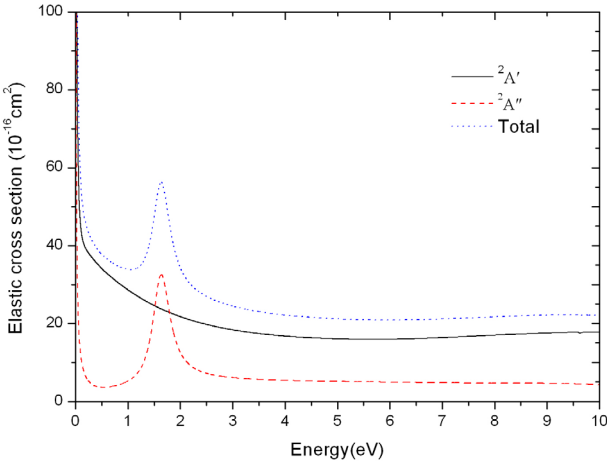

Fig. 1. Elastic cross sections of the electron impact on the methyleneimine molecule in the SEP model. Solid curve: $^2A''$ component; dashed curve: $^2A'$ component; dash-dotted curve: total cross section.

3 Results

3.1 Static-exchange-polarization scattering calculations

The elastic cross sections of electron collision with H_2CNH in SEP model based on the 6-31G basis set are shown in Figure 1. The total cross section shows a broad peak at 1.65 eV. We find that the resonance peak at 1.65 eV comes from the $^2A''$ symmetry. This resonance is usually called π^* resonance since the incident electron is captured in a virtual π^* MO of H_2CNH. It is noted that the A'' symmetry has angular momentum barrier and the integrate cross section usually vanish at zero energy. But for the present polar molecule, a large dipole potential can overcome the centrifugal barrier, and the elastic cross section of $^2A''$ symmetry shows rapid rise at low energy This is the reason why it is necessary to add the Born correction to dipolar system This phenomenon was also discussed before [23].

3.2 Close-coupling scattering calculations

The elastic cross sections calculated in ten states CC model are shown in Figure 2. We find there is a broad peak at 1.95 eV in the total elastic cross section profile. Carefully analyzing the two components ($^2A''$ and $^2A''$) of the total elastic cross section, we find that the resonance around 1.95 eV comes from $^2A''$ symmetry The resonance parameters (the energy position and the width of the resonance) can (in most cases) be determined by fitting the eigenphase sum to a Breit-Wigner profile [24,25]. All resonances revealed in the present calculations are presented in Table 2, together with the values of the resonance parameters. The resonance around 1.95 eV in $^2A''$ symmetry is a $\pi*$ shape resonance with a width of 0.56 eV. Since the numbers of virtual orbitals and double-electron excitations are fewer than that used in the SEP calculations,

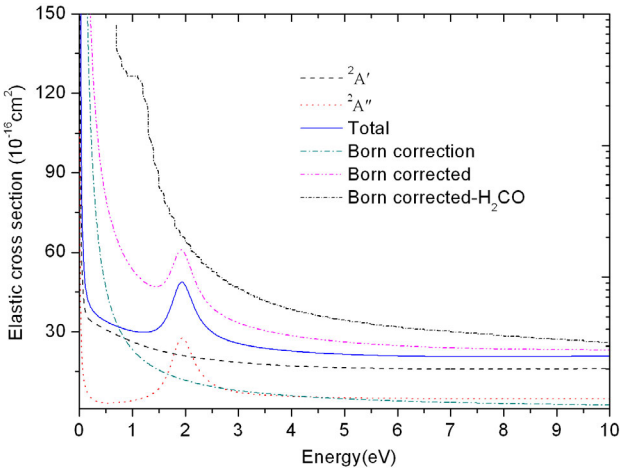

Fig. 2. Elastic cross sections of the electron impact on the methyleneimine molecule in the CC model together with the elastic cross section of H_2CO form reference [28]. Dashed curve: $^2A'$ component; dotted curve: $^2A''$ component; solid curve; total cross sections; dash-dotted curve: Born correction cross section; dashed double-dotted curve: Born corrected cross section; short-dash-dotted curve: elastic cross section of H_2CO form reference [27].

Table 2. Shape resonance of the electron-H_2CNH scattering system.

Type	Configuration	Position (eV)	Width (eV)
SEP	$(1^1A')\ 2a''^1$	1.65	0.41
CC	$(1^1A')\ 2a''^1$	1.95	0.56

the π^* resonance predicted in the CC model is slightly higher in energy than that in the SEP model. To obtain converged cross sections, the effect of rotation must be included along with a very large number of partial waves. The effects of partial waves with $l > 4$ were included using a Born correction via a closure approach [26,27]. The summed elastic integral cross section including the Born correction is also shown in Figure 2. We have presented the elastic cross section of electron impact on H_2CO molecule from reference [28] for comparison in Figure 2. Although they are isoelectronic molecules, the cross section of H_2CO is higher than that of H_2CNH due to its stronger polarity.

3.3 Differential cross section

A more stringer test for any theoretical model is to calculate the DCS. The DCS for a general polyatomic molecule is given by:

$$\frac{d\sigma}{d\Omega} = \sum_L A_L P_L(\cos\theta), \tag{2}$$

where P_L is a Legendre function. The A_L coefficients have been discussed in detail before [29]. For a polar molecule this expansion over L converges slowly. In order to accelerate the convergence of DCS, the following

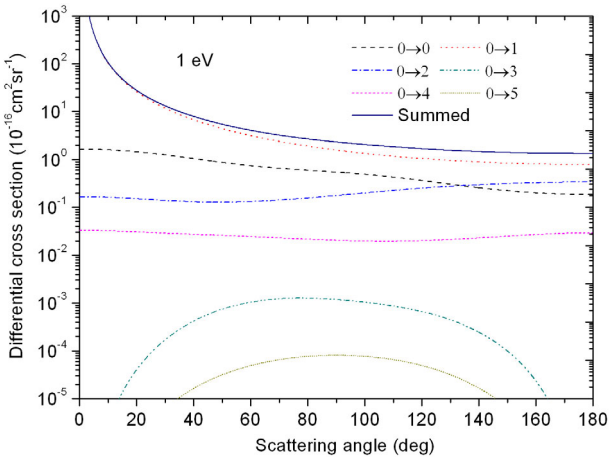

Fig. 3. Electron impact R-matrix rotationally resolved state-to-state ($J \to J'$) differential cross sections of H_2CNH at 1 eV. dashed curve: $J = 0 \to J' = 0$; dotted curve: $J = 0 \to J' = 1$; dash dotted curve: $J = 0 \to J' = 2$; dash double dotted curve: $J = 0 \to J' = 3$; short dashed curve: $J = 0 \to J' = 4$; short dotted curve: $J = 0 \to J' = 5$; solid curve: summed.

closure formula is used,

$$\frac{d\sigma}{d\Omega} = \frac{d\sigma^B}{d\Omega} + \sum_L \left(A_L - A_L^B\right) P_L(\cos\theta). \tag{3}$$

The superscript B represents the relevant quantity which is calculated in the Born approximation with an electron-point dipole interaction. The convergence of the summation over L in equation (5) is now rapid because the contribution from the higher partial waves to the DCS is dominated by electron-dipole interaction. The quantity $d\sigma^B/d\Omega$ for any initial rotor state $|J\tau\rangle$ is given by the sum over all the final rotor states $|J'\tau'\rangle$

$$\frac{d\sigma^B}{d\Omega} = \sum_{J'\tau'} \frac{d\sigma^B}{d\Omega}(J\tau \to J'\tau'). \tag{4}$$

The expressions for the state-to-state rotationally inelastic DCS, $d\sigma^B/d\Omega\,(J\tau \to J'\tau')$, for a spherical top, a symmetric top, and asymmetric top molecules have been given by Sanna and Gianturco [30]. The calculated dipole moment (1.76 D), the experimental dipole moment (2.00 D) [17] and rotational constants ($A = 6.6104$ cm^{-1}, $B = 1.1642$ cm^{-1}, and $C = 0.9899$ cm^{-1}) [17] for H_2CNH are used in the calculations of the DCSs ($J = 0 \to J' = 0, 1, 2, 3, \ldots$).

Our calculated rotationally resolved DCSs for electron scattering by H_2CNH at the incident energy of 1 eV are shown in Figure 3. Due to strong polar nature of H_2CNH molecule, the $0 \to 1$ contribution is bigger than the elastic $0 \to 0$ component, especially at the low angles Therefore the dominant feature of the state-resolved DCS is the dipole component $0 \to 1$. As shown in the figure, the contribution of the higher J' decreases with the J' increases, and the convergent results are obtained when J' increases up to 5. The DCSs obtained by summarizing the rotational

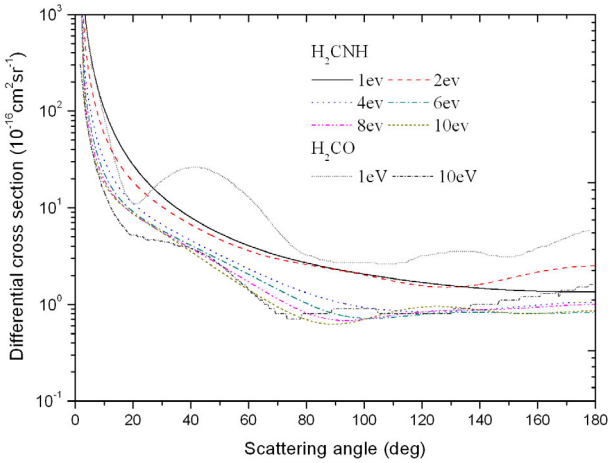

Fig. 4. Differential cross section (DCS) of H_2CNH at different energies 1, 2, 4, 6, 8 and 10 eV and DCS of H_2CO at 1 and 10 eV from reference [27]. For H_2CNH, solid curve: 1 eV; dashed curve: 2 eV; dotted curve: 4 eV; dash dotted curve: 6 eV; dash double dotted curve: 8 eV; short dashed curve: 10 eV. For H_2CO, short-dotted curve: 1 eV; short-dash-dotted curve: 10 eV.

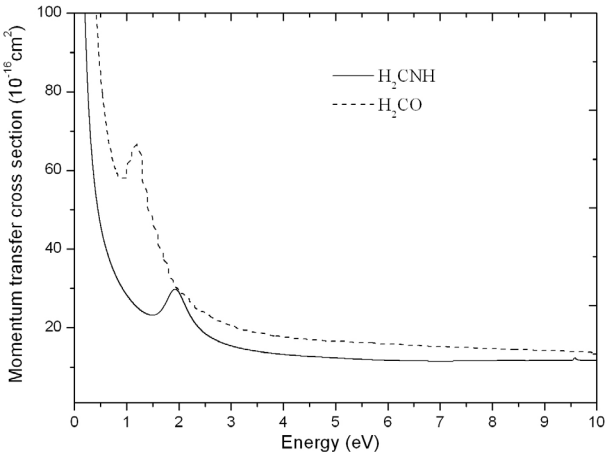

Fig. 5. Momentum transfer cross sections of H_2CNH and H_2CO for energy range of 0.01−10.00 eV.

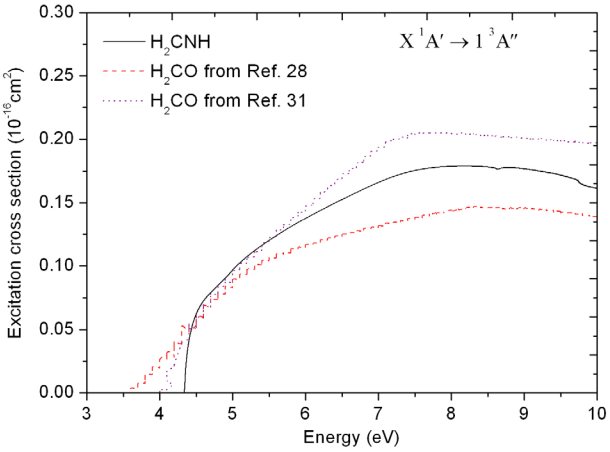

Fig. 6. Comparison Electron-impact excitation cross sections from the ground state X^1A' (X^1A_1) to the $1^3A''$ (1^3A_2) of H_2CNH with H_2CO. Solid line: $X^1A' \rightarrow 1^3A''$ of H_2CNH; dashed line: $X^1A_1 \rightarrow 1^3A_2$ of H_2CO from reference [28]; dotted line: $X^1A_1 \rightarrow 1^3A_2$ of H_2CO from reference [31].

cross sections for ($J = 0 \rightarrow J' = 0 \sim 5$) at the selected energies of 1, 2, 4, 6, 8 and 10 eV are depicted in Figure 4. Due to the dipolar nature of the target, the DCSs at all the energies show the sharp increases at the smaller scattering angles. The DCS at 2 eV appears a minimum at about 130°. The minimum of the DCS reduces to 90° with the incident energy increasing to 10 eV. Although there is no experimental DCS available for comparison, theoretical DCS results of H_2CO calculated by Kaur and Baluja [28] using R-matrix method are available at 1 eV and 10 eV, which are also shown in Figure 4. Comparing with H_2CNH, the DCS of H_2CO at 1 eV appears an obvious hump and is larger in the scattering angles >30°. For the DCS at 10 eV, both of them have the similar shape in general.

By using the POLYDCS program, the momentum transfer cross sections (MTCS) are calculated and presented in Figure 5. We observe the MTCS decreases with the increasing energy. In contrast to the diverging nature of DCS in the forward direction (at the small scattering angles), MTCS show no singularity due to the multiplicative factor $(1-\cos\theta)$, where θ is scattering angle. It is obvious that the π^* shape resonance at 1.95 eV is responsible for the peaks observed at around 1.95 eV in the MTCS. The MTCS indicates the weights of backward-scattering and is useful in the study of electrons drifting through a molecular gas. In Figure 5, we have shown a comparison of the calculated MTCSs for the H_2CNH and H_2CO [28]. As shown in the figure, the MTCS for H_2CO are higher than their corresponding values for the H_2CNH molecule.

3.4 Inelastic cross sections

Not only the elastic cross sections, but also the electronic excitation cross sections are very important to astrophysics and plasmas physics. For there is no experimental and theoretical inelastic cross sections available, the present data is essential and must be regarded as predictive. The electronic excitation cross section from the ground state X^1A' to the first three excited state $1^3A''$, $1^3A'$ and $1^1A''$ is shown in Figures 6, 7 and 8, respectively. It is noted that the electron transitions to the $1^3A''$ and $1^3A'$ states are spin forbidden, while only the transition $X^1A' \rightarrow 1^1A''$ is optically allowed. In Figure 6 we have shown the comparison of the $X^1A' \rightarrow 1^3A''$ transition of H_2CNH molecule with H_2CO calculated by R-matrix method [28] and Schwinger variational method [31]. The cross section of H_2CO from reference [30] is higher than the other two R-matrix results as they have neglected close channel effects which are expected to lower the cross sections. And this has been discussed in reference [28]. Figure 7 depicts the comparison of the $X^1A' \rightarrow 1^3A'$ of H_2CNH molecule with H_2CO calculated by R-matrix

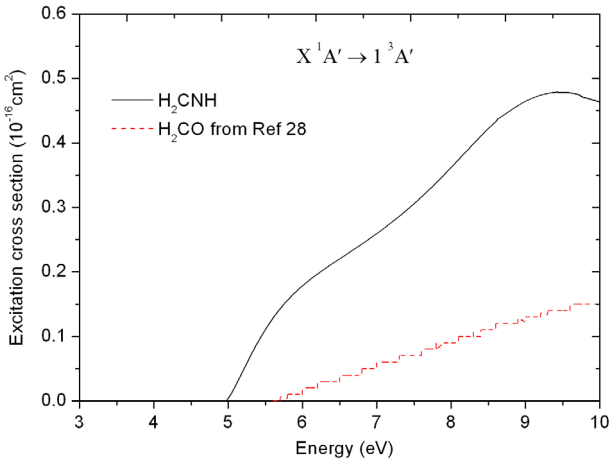

Fig. 7. Comparison of electron-impact excitation cross sections from the ground state X^1A' (X^1A_1) to the $1^3A'$ (1^3A_1) of H_2CNH with H_2CO. Solid line: $X^1A' \rightarrow 1^3A'$ of H_2CNH; dashed line: $X^1A_1 \rightarrow 1^3A_1$ of H_2CO from reference [28].

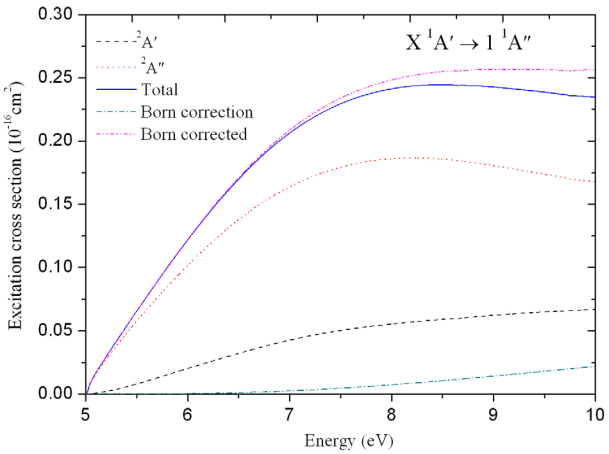

Fig. 8. Electron-impact excitation cross sections from the ground state X^1A' to the $1^1A''$ state. Dashed line: $^2A'$; dotted line: $^2A''$; solid line: total; dash dotted curve: Born correction; dash double-dotted curve: Born corrected.

method [28]. It is obvious that the cross section of H_2CNH is higher than that of H_2CO.

Figure 8 depicts the optically allowed $X^1A' \rightarrow 1^1A''$ excitation cross section. The cross section for the transition has been Born corrected [18,19]. As shown in the figure, the Born correction cross section increases as the incident electron increases. The contribution of the $^2A''$ symmetry is also larger than that of the $^2A'$ symmetry.

3.5 Effective collision frequency of electrons

Two types of the effective electron-H_2CNH collision frequency $\langle\nu\rangle$ and $\overline{\nu}$ (see Baille et al. [32]) are evaluated based on the MTCS data in the present work. These are given by the following expressions, in which it is assumed that the electrons follow a Maxwell-Boltzmann distribution:

$$\langle\nu\rangle = \frac{8}{3\pi^{1/2}} N \left(\frac{m_e}{2KT_e}\right)^{5/2} \int_0^\infty \nu^5 Q^m(V) e^{-\frac{m_e\nu^2}{2KT_e}} d\nu,$$

$$\overline{\nu}^{-1} = \frac{8}{3\pi^{1/2}N} \left(\frac{m_e}{2KT_e}\right)^{5/2} \int_0^\infty \frac{\nu^3}{Q^m(\nu)} e^{-\frac{m_e v^2}{2KT_e}} d\nu.$$

Here, N is the number density of molecules, m_e is the electron mass, k is the Boltzmann factor, T_e is the electron temperature, v is the velocity of the electron, and $Q^m(v)$ is the velocity-dependent MTCS. These are plotted in Figure 9. These collision frequencies are related to transport properties like mean-free path, mobilities, and diffusion coefficients. These find applications in the study of electrons swarming through molecular gases.

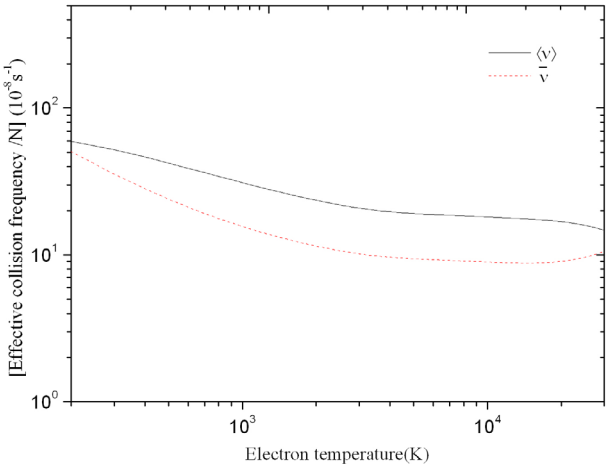

Fig. 9. Effective collision frequency of the H_2CNH molecule ground state: solid curve, $\langle\nu\rangle$; dashed curve, $\overline{\nu}$.

4 Conclusion

The elastic cross sections of low-energy electron collision with H_2CNH molecule are calculated using the R-matrix method within the SEP and CC approximations. The inelastic excitation cross sections are also calculated within the CC approximation. We detect a π^* shape resonance of $^2A''$ symmetry located at 1.95 eV with a width of 0.56 eV within CC approximation. This shape resonance is also observed in the MTCS of H_2CNH. The effective electron-H_2CNH collision frequency which is used to evaluation of transport coefficients is also calculated. For there is no experimental cross sections available for H_2CNH molecule, the present calculations must be regarded as predictive.

This work is partially supported by Henan fundamental and advanced research project (No. 142300410022), the Foundation of Henan Educational Committee (Nos. 2011A140015 and 12A140006) and National Development Fund of Henan Normal University (No. 2012PL02).

References

1. D.L. Huestis, S.W. Bougher, J.L. Fox, M. Galand, R.E. Johnson, J.I. Moses, J.C. Pickering, Space. Sci. Rev. **139**, 63 (2008)
2. A. Luque, U. Ebert, W. Hundsdorfer, Phys. Rev. Lett. **101**, 075005 (2008)
3. J.M. Ajello, D.E. Shemansky, W.R. Pryor, A.I. Stewart, K.E. Simmons, T. Majeed, J.H. Waite, G.R. Gladstone, D. Grodent, Icarus **152**, 151 (2001)
4. W.D. Geppert, M. Larsson, Mol. Phys. **106**, 2199 (2008)
5. A. Fuente, S. Garca-Burillo, A. Usero, M. Gerin, R. Neri, A. Faure, J.L. Bourlot, M. Gonzalez-Garcia, J.R. Rizzo, T. Alonso-Albi, J. Tennyson, A&A **492**, 675 (2008)
6. M. Roellig, N.P. Abel, T. Bell, F. Bensch, J. Black, G.J. Ferland, B. Jonkheid, I. Kamp, M.J. Kaufman, J.L. Bourlot, F.L. Petit, R. Meijerink, O. Morata, V. Ossenkopf, E. Roueff, G. Shaw, M. Spaans, A. Sternberg, J. Stutzki, W.-F. Thi, E.F. van Dishoeck, P.A.M. van Hoof, S. Viti, M.G. Wolfire, A&A **467**, 187 (2007)
7. B. Boudaïffa, P. Cloutier, D. Hunting, M.A. Huels, L. Sanche, Science **287**, 1658 (2000)
8. P.D. Godfrey, R.D. Brown, B.J. Robinson, M.W. Sinclair, Astrophys. Lett. **13**, 119 (1973)
9. J.E. Dickens, W.M. Irvine, C.H. DeVries, M. Ohishi, Astrophys. J. **479**, 307 (1997)
10. R.V. Yelle, V. Vuitton, P. Lavvas, S.J. Klippenstein, M.A. Smith, S.M. HÖrst, J. Cui, Faraday Discuss. **147**, 1 (2010)
11. Y. Lee, C-.J. Tang, T.A. Litzinger, Combust. Flame **117**, 600 (1999)
12. J.M. Carr, P.G. Galiatsatos, J.D. Gorfinkiel, A.G. Harvey, M.A. Lysaght, D. Madden, Z. Masin, M. Plummer, J. Tennyson, H.N. Varambhia, Eur. Phys. J. D **66**, 58 (2012)
13. J. Tennyson, Phys. Rep. **491**, 29 (2010)
14. P.G. Burke, *R-Matrix Theory of Atomic Collisions: Application to Atomic, Molecular and Optical Processes* (Springer-Verlag, Berlin, 2011)
15. L.A. Morgan, C.J. Gillan, J. Tennyson, X. Chen, J. Phys. B **30**, 4087 (1997)
16. B.M. Nestmann, K. Pfingst, S.D. Peyerimhoff, J. Phys. B **27**, 2297 (1994)
17. NIST, Computational chemistry comparison and benchmark database, http://cccbdb.nist.gov/ (2008)
18. R. Cimiraglia, J. Tomasi, J. Am. Chem. Soc. **99**, 1135 (1972)
19. P.J. Bruna, V. Krumbach, S.D. Peyerimhoff, Can. J. Chem. **63**, 1594 (1985)
20. R. Sumathi, J. Mol. Struct. **364**, 97 (1996)
21. R. Ditchfield, J.E.D. Bene, J.A. Pople, J. Am. Chem. Soc. **94**, 703 (1972)
22. A. Faure, J.D. Gorfinkiel, L.A. Morgan, J. Tennyson, Comput. Phys. Commun. **144**, 224 (2002)
23. A. Dora, J. Tennyson, L. Bryjko, T. van Mourik, J. Chem. Phys. **130**, 164307 (2009)
24. J. Tennyson, C.J. Noble, Comput. Phys. Commun. **33**, 421 (1984)
25. H. Friedrich, *Theoretical Atomic Physics*, 3rd edn. (Springer, Berlin, 2006), p. 47
26. S. Kaur, K.L. Baluja, J. Tennyson, Phys. Rev. A **77**, 032718 (2008)
27. S. Kaur, K.L. Baluja, Phys. Rev. A **80**, 042701 (2009)
28. S. Kaur, K.L. Baluja, J. Phys. B **38**, 3917 (2005)
29. F.A. Gianturco, A. Jain, Phys. Rep. **143**, 347 (1986)
30. N. Sanna, F.A. Gianturco, Comput. Phys. Commun. **114**, 142 (1998)
31. Q.Y. Sun, C. Winstead, V. McKoy, Phys. Rev. A **46**, 2462 (1992)
32. P. Baille, J.S. Chang, A. Claude, R.M. Hobson, G.L. Ogram, A.W. Yau, J. Phys. B **14**, 1485 (1981)